ACS OMEGA

Article

Cite This: ACS Omega 2018, 3, 8017−8026

Development of Doxorubicin-Loaded Magnetic Silica−Pluronic F-127 Nanocarriers Conjugated with Transferrin for Treating Glioblastoma across the Blood−Brain Barrier Using an in Vitro Model

Geetha B. Heggannavar,[†] Chinmay G. Hiremath,[†] Divya D. Achari,[†] Vishwas G. Pangarkar,[‡] and Mahadevappa Y. Kariduraganavar*[,†]

[†]Department of Studies in Chemistry, Karnatak University, Dharwad 580 003, India

[‡]Institute of Chemical Technology, Matunga, Mumbai 400 019, India

ABSTRACT: Brain glioma is the most lethal type of cancer, with extremely poor prognosis and high relapse. Unfortunately, the treatment of brain glioma is often limited because of the low permeability of anticancer drugs across the blood−brain barrier (BBB). To circumvent this, magnetic mesoporous nanoparticles were synthesized and loaded with doxorubicin as an anticancer agent. These nanoparticles were fabricated with Pluronic F-127 and subsequently conjugated with transferrin (Tf) to achieve the sustained release of the drug at the targeted site. The physicochemical properties of the conjugated nanoparticles were analyzed using different techniques. The magnetic saturation of the nanoparticles determined by a vibration sample magnetometer was found to be 26.10 emu/g. The cytotoxicity study was performed using the MTT assay at 48 and 96 h against the U87 cell line. The Tf-conjugated nanoparticles (DOX-MNP-MSN-PF-127-Tf) exhibited a significant IC_{50} value (0.570 μg/mL) as compared to the blank nanoparticles (121.98 μg/mL). To understand the transport mechanism of drugs across the BBB, an in vitro BBB model using human brain microvascular endothelial cells was developed. Among the nanoparticles, the Tf-conjugated nanoparticles demonstrated an excellent permeability across the BBB. This effect was predominant in the presence of an external magnetic field, suggesting that magnetic particles present in the matrix facilitated the uptake of drugs in U87 cells. Finally, it is concluded that nanoparticles conjugated with Tf effectively crossed the BBB. Thus, the developed nanocarriers can be considered as potential candidates to treat brain tumor.

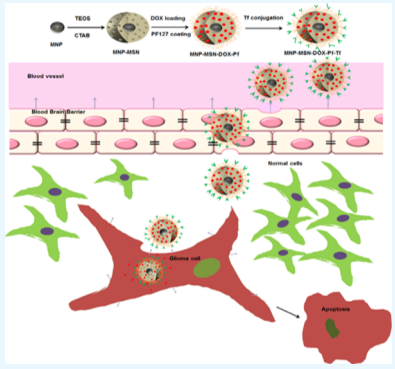

1. INTRODUCTION

Glioblastoma multiforme is a malignant glial tumor and a commonly occurring type of primary astrocytomas. It accounts for more than 60% of all brain tumors in adults.[1] Patients usually have a less survival rate of approximately 14 to 15 months after diagnosis.[2,3] Even with advances in treatment modalities, it remains largely incurable because of the presence of complexities associated with the target-specific treatment across the blood−brain barrier (BBB). The structure of the BBB involves the complex design of tight junctions between the endothelial cells. These cells are known to express the efflux transport proteins, which maintain the homeostasis of the central nervous system (CNS) by controlling the transport of substances into the brain.[4,5]

Recently, nanotechnology has shown an immense application in cancer-targeted therapy.[6−9] Cancer-targeted nano drug-delivery systems are particularly expected to enhance the anticancer activity while minimizing the side effects, and thus showing an excellent potential application in cancer therapy.[10−12] There are various biocompatible materials that have created a tremendous curiosity in cancer therapy, viz., silica nanoparticles (NPs),[13,14] nanoliposomes,[15] and magnetic NPs (MNPs).[16] With certain modifications in these materials, we can prolong the drug's half-life, increase its viability in the blood circulation, and allow the specific cell-targeting properties. To address this, Chen et al.[17] developed a magnetic drug-delivery system in which doxorubicin (DOX) was chemically bonded to Fe_3O_4 NPs, and it was then embedded in polyethylene glycol (PEG) to functionalize the porous silica shell. Similarly, Guan et al.[18] developed a multitargeted oleic acid (OA)−MNPs and demonstrated an excellent in vivo and in vitro efficacy in treating the human cervical cancer HeLa cells. These studies concluded that MNPs loaded with effective antitumor drugs offered physical therapy, which has advantages over the other nonloaded drugs, such as small particle size, large specific surface, high-capacity coupling, and good magnetic response. With these possibilities, one can overcome the drawbacks of the conventional treatment strategies.[19−21] The mesoporous silica NPs are likely to play an important role for designing the drug carriers that plague cancer therapy

Received: January 24, 2018
Accepted: July 5, 2018
Published: July 18, 2018

DOI: 10.1021/acsomega.8b00152
ACS Omega 2018, 3, 8017−8026

because of their low toxicity, biocompatibility, controllable particle size and pore morphologies, and facile surface decoration.[22−26] While modifying the MNPs, surface functionalization is also an important strategy, which can be achieved by choosing the appropriate species, such as polymers, surfactants, and biomolecules.[27,28] Pluronic copolymer is especially promising for the modification of NPs. Pluronic F-127 is an FDA-approved biocompatible and thermoreversible block copolymer, which contains poly(ethylene oxide)−poly(propylene oxide)−poly(ethylene oxide) blocks. Wei et al.[29] developed micelles to combat the multidrug resistance (MDR) using Pluronic P-123 (PP-123) and Pluronic F-127 (PF-127). Owing to the sensitizing properties of PP-123 and the long circulation effect of PF-127, the micelles could be able to enhance the activity of paclitaxel to overcome the MDR in lung cancer. Pluronic micelles have also been studied to bypass the BBB for drug delivery to the CNS.[30] In the past few years, it has been found that the modification of drug-delivery carriers with targeting ligands can improve the transport efficiency across the BBB.[31−34] Recently, it has been reported that a high level of Tf receptors (Tf-Rs) was expressed in brain capillary endothelial cells and glioma cells involved in receptor-mediated transcytosis through the BBB.[35,36] These receptors could be targeted with the corresponding ligands. Consequently, Tf crosses the intact BBB freely, which helps to carry the essential nutrients into the brain.

Understanding the pros and cons of the aforesaid materials and the strategies adopted, we have synthesized the functionalized magnetic mesoporous NPs loaded with DOX as an anticancer agent. These NPs were carefully fabricated with PF-127 and subsequently conjugated with Tf to promote its infiltration across the BBB and also for achieving the sustained release of the drug at the targeted site. The physicochemical properties of the resulting NPs were evaluated with different techniques. The size and shape of the NPs were determined using dynamic light scattering (DLS) and transmission electron microscopy (TEM). The retention of magnetic property subsequent to the coating of silica and the polymer on the developed NPs was tested using a vibrating sample magnetometer. The cytotoxicity study was carried out using MTT assay after 48 and 96 h of treatment against the U87 cell line. A BBB model with human brain microvascular endothelial (HBME) cells was developed to study the passage of drugs across the barrier. Among the carriers developed, the Tf-conjugated carriers demonstrated an excellent permeability across the barrier through receptor-mediated transcytosis. This behavior was predominant in the presence of magnetic field, as evidenced by the data.

2. RESULTS AND DISCUSSION

2.1. Synthesis and Characterization of Nanocarriers.

The present work was focused to design and develop the temperature-responsive polymer nanocarriers for the targeted delivery of an anticancer DOX drug to achieve an enhanced anticancer activity against glioma cells. The stepwise preparation of magnetic mesoporous nanocarriers is shown in Schemes 1−6. The MNPs were synthesized by an aqueous co-precipitation approach in the presence of ammonia. To create the pores for drug loading, the mesoporous magnetic silica NPs were prepared using triethylorthosilicate (TEOS) along with decane and 1,3,5-triisopropylbenzene (TIPB) as pore swelling agents. Further, these were functionalized with amino groups using (3-aminopropyl)triethoxysilane

Scheme 1. Preparation of MNPs

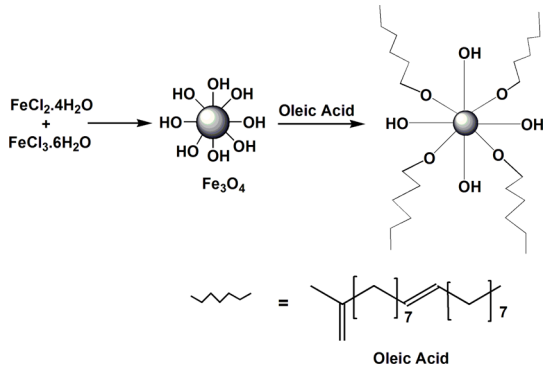

Scheme 2. Preparation of Mesoporous Silica MNPs

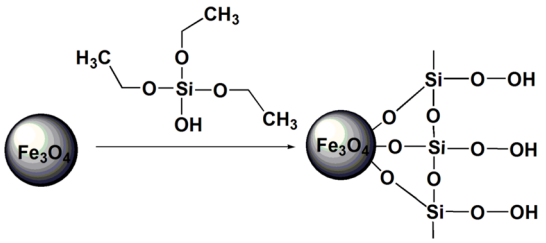

Scheme 3. Preparation of Drug-Loaded NPs and Their Amine Functionalization

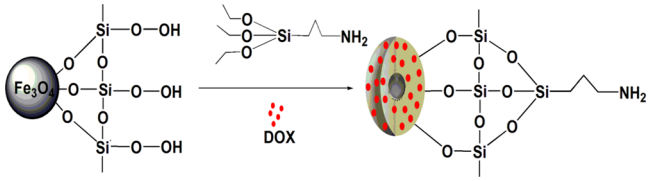

Scheme 4. End Group Modification of Pluronic F-127

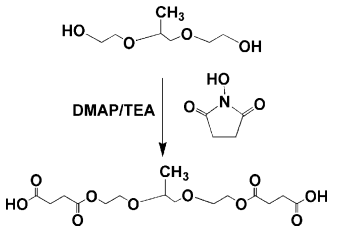

(APTES). PF-127 was chosen as it is known to bypass the BBB. In addition to this, it is also known as a thermoresponsive polymer because of its lower critical solution temperature (LCST), which facilitates the formation of self-assembly around the body temperature.[37] Before conjugating the MNP-MSN, the end groups (−OH) of PF-127 were modified with the −COOH group using succinic anhydride (SA). The amino groups present on the surface of MNP-MSN were then covalently attached to the −COOH group of PF-127 via the 1-ethyl-3-(3-dimethylaminopropyl)carbodiimide hydrochloride/*N*-hydroxysuccinimide (EDC/NHS) approach. The permeation of drugs across the BBB and cancer-targeting properties were introduced in this synthesized MNP-MSN-PF-127 through the conjugation of Tf.

The Fourier transform infrared (FTIR) spectra of OA-MNP, MNP-MSN, MNP-MSN-NH_2, PF-127, modified PF-127 (MPF-127), MNP-MSN-MPF-127, Tf, and MNP-MSN-

DOI: 10.1021/acsomega.8b00152
ACS Omega 2018, 3, 8017−8026

Scheme 5. Conjugation of Pluronic F-127 with DOX-MNP-MSN-NH_2

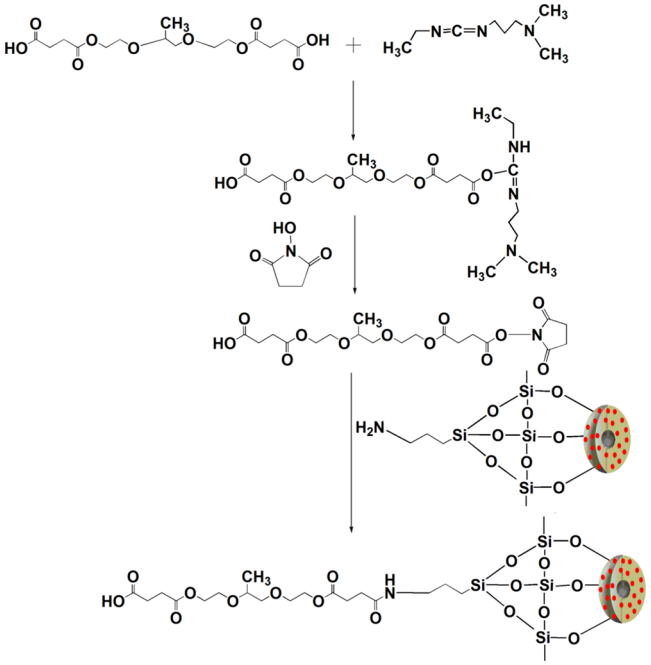

Scheme 6. Conjugation of Tf on the Surface of the Drug-Loaded NPs

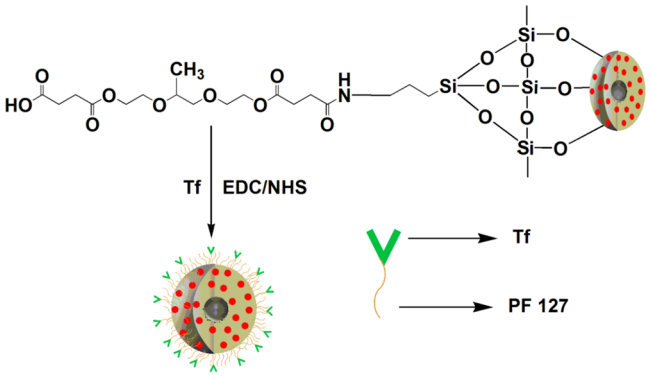

MPF-127-Tf were recorded in the range of 400−4000 cm^{-1}. All the bands showed expected stretching, indicating that the preparation of MNPs and their stabilization with OA and mesoporous silica NPs with TEOS; functionalization of mesoporous silica NPs with APTES; and modification of PF-127 with SA, MNP-MSN-PF-127, and Tf-conjugated MNP-MSN-PF-127 were successfully achieved. However, the spectra of these are not included to minimize the number of figures. Only the representative spectra such as those of MNP-MSN-PF-127, Tf, and MNP-MSN-PF-127-Tf are presented in Figure 1. The bands that appeared at around 1560 and 1650 cm^{-1} in the spectrum of MNP-MSN-PF-127 are respectively attributed to the stretching and deformation vibrations of the amide bonds that are covalently bonded between PF-127 and MNP-MSN-NH_2. The Tf exhibited bands at around 1280, 1530, and 1660 cm^{-1}, and these are respectively assigned to amide III, amide II, and amide I. The intensity of these bands decreased significantly owing to the reaction that occurred between amide groups of Tf and −COOH groups of PF-127. This

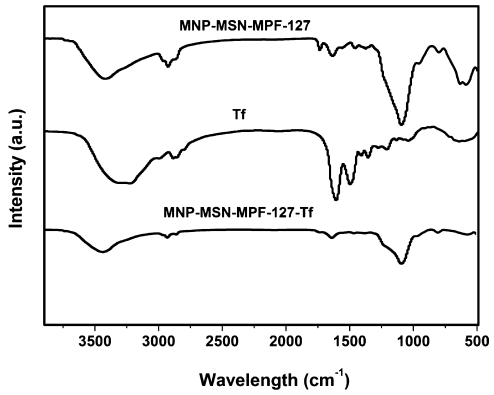

Figure 1. FTIR spectra of MNP-MSN-MPF-127, Tf, and MNP-MSN-MPF-127-Tf.

suggests that Tf was successfully conjugated on the surface of MNP-MSN-PF-127.

To know the distribution of the hydrodynamic size of the resulting nanocarriers, the dispersed NPs in water were analyzed in a zeta-sizer using the DLS technique. The resulting data are presented in Figure 2. The data revealed that the

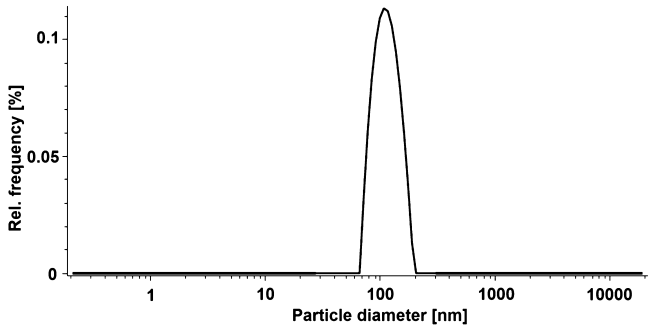

Figure 2. Histogram of DLS of MNP-MSN-PF-127.

hydrodynamic size of the nanocarriers was approximately 159 nm. Further, to know the physical stability of the colloidal dispersions, the zeta potential was measured and was found to be −26.3 mV. This suggests that carriers developed in the present study have a relatively narrow size distribution, better dispersity, and stability in aqueous solution. The synthesized magnetic mesoporous silica NPs and their resulting conjugation with PF-127 before drug loading were subjected to TEM by carefully depositing them on a copper grid. The images thus obtained are presented in Figure 3. From the image of MNP-MSN, it is observed that the size of the particles was mainly in the range of 60−80 nm, with an iron oxide

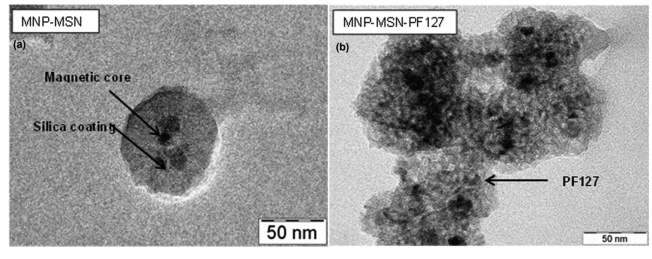

Figure 3. TEM images of (a) MNP-MSN and (b) MNP-MSN-PF-127.

DOI: 10.1021/acsomega.8b00152
ACS Omega 2018, 3, 8017−8026

nanocrystal core located at the center. The observed mesoporous structure was also supported by the nitrogen adsorption−desorption isotherms, which demonstrated that MNP-MSNs have a uniform pore size distribution of around 2.66 nm. However, when these particles were conjugated with PF-127, the size of the particles was increased to 110 nm. This can be attributed to the presence of a thin polymer coating on the surface of MNP-MSN. This clearly ascertains the successful modification of NPs with PF-127. However, some agglomeration was also observed in both the images, and this might be due to their magnetization energy.

The thermogravimetric analyses of magnetic mesoporous silica NPs and their conjugation with PF-127 are shown in Figure 4. It is observed that in both the thermograms, the

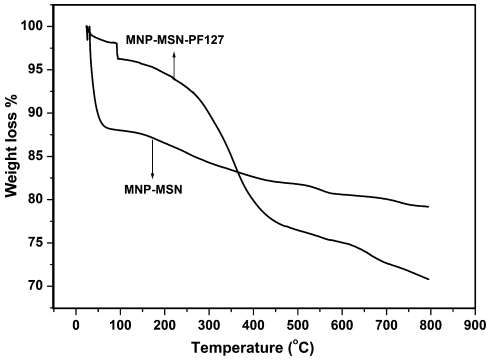

Figure 4. Thermogravimetric analysis (TGA) thermograms of MNP-MSN and MNP-MSN-PF-127.

weight loss was observed in three stages. The first weight loss was observed up to 100 °C in both the thermograms and is mainly because of the loss of adsorbed water molecules. PF-127-coated NPs exhibited relatively low weight loss of 4 wt %. On the contrary, magnetic mesoporous NPs exhibited a higher weight loss of about 12 wt %. This indicates that the mesoporous NPs have a higher hydrophilic character owing to the presence of −OH groups. In the second stage (100−500 °C), the weight loss was significant for PF-127-coated mesoporous NPs, which corresponds to around 20 wt %. This is mainly due to the weight loss of PF-127. For mesoporous NPs, it is about 7 wt %, which corresponds to the weight loss of mesoporous silica. Further weight loss was observed beyond 500 °C in both the cases because of the oxidation of MNPs. From the thermograms, it was also observed that PF-127-coated NPs were relatively more stable than magnetic mesoporous NPs. On the basis of the evidence, we can conclude that the resulting PF-127-coated NPs have an adequate thermal stability with a sufficient polymer coating, suggesting that the coated amount of PF-127 is enough to get the compatibility and dispersity for the controlled delivery of drugs.

To authenticate the feasibility and sensitivity of the developed NPs as targeted contrast agents, it is important to retain the favorable magnetic property of the NPs after the surface modification. Accordingly, the magnetization property of the OA-stabilized NPs (OA-MNP) and MNP-MSN-PF-127 NPs was determined at room temperature using a vibration sample magnetometer (VSM). The data thus obtained are presented in Figure 5.

Both the samples did not show coercivity forces, indicating that both have a good superparamagnetism property with no

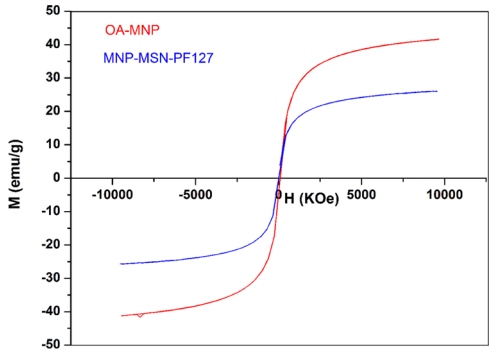

Figure 5. Magnetization curve of OA-MNP and MNP-MSN-PF-127.

remnant magnetization and hysteresis. For OA-MNP, the saturation magnetism (M_s) was found to be 41.7 emu/g. However, the saturation magnetism of MNP-MSN-PF-127 was found to be 26.1 emu/g. The results suggest that after the modification with silica and PF-127, the MNP-MSN-PF-127 exhibited a superparamagnetic nature with reduced magnetization compared to OA-MNP, signifying their successful modification. Evidently, the particles developed here (MNP-MSN-PF-127-Tf) would certainly contribute to a stronger responsiveness against the magnetic field. Thus, the resulting carriers could be guided to a specific tumor site efficiently with an enhanced therapeutic effect. During the synthesis of MNP-MSNs, the swelling agents such as decane and TIPB were employed to create pores in the NPs so as to improve the drug-loading capacity. The nitrogen gas adsorption−desorption isotherms and pore size distribution of the mesoporous silica NPs are presented in Figure 6A,Brespectively.

The pore size distribution obtained from the isotherms after the eviction of CTAB from MNP-MSN was determined using the Barrett−Joyner−Halenda (BJH) method. The CTAB is known to dictate the structure of the pore size. On the basis of the nature of the plot, it was found that the resulting MNP-MSN NPs demonstrated type IV adsorption−desorption isotherms, and Figure 6A resembles H1 hysteresis occurring from P/P_0, which is associated with the presence of uniform mesopores. Similarly, using the Brunauer−Emmett−Teller (BET) equation, the specific surface area and pore volume of the MNP-MSN NPs were determined as ∼257.4 m^2/g and 0.53 cm^3/g, respectively. The pore diameter of the magnetic mesoporous silica NPs as determined by the peak of Figure 6B was found to be ∼2.66 nm.

2.2. Encapsulation Efficiency and in Vitro Release of Drugs. One of the important characteristics of the drug-delivery system in the field of biomedicine is to impart the sustained release of drug. Generally, an ideal drug carrier should possess enhanced encapsulation efficiency (EE) and a high drug-loading ability. To study this, the drug was loaded into MNP-MSN-PF-127-Tf NPs and the percentage of drug-loading capacity and EE was determined. It was found that the loading capacity and EE of DOX in MNP-MSN were 36.88 and 92.2%, respectively. After the modification with PF-127 and Tf, the loading capacity and EE of DOX were found to be 34.6 and 86.5%, respectively. The in vitro drug release study was performed by dispersing the drug-loaded NPs (MNP-MSN-PF-127-DOX-Tf) in a phosphate-buffered saline (PBS) solution of pH 7.4 containing 0.05% (w/v) of Tween 80. To understand the thermoresponsive behavior of the NPs, the release profile of DOX-loaded NPs under the influence of

DOI: 10.1021/acsomega.8b00152
ACS Omega 2018, 3, 8017−8026

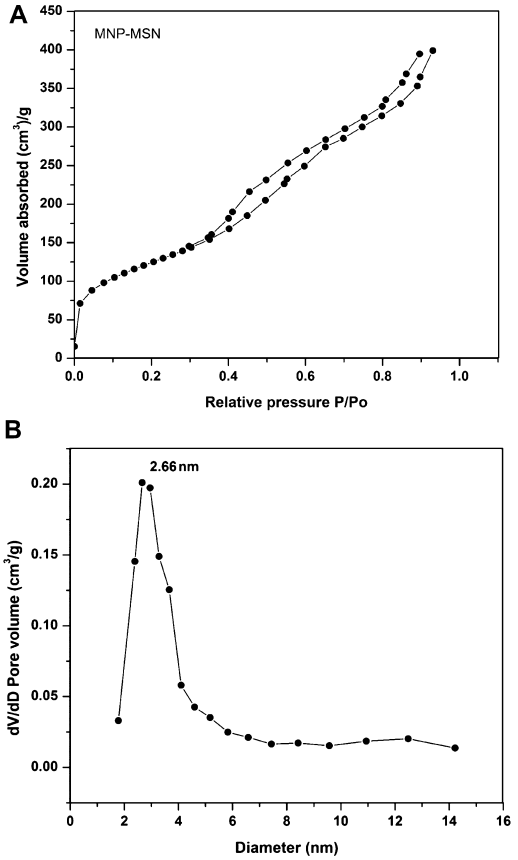

Figure 6. (A) Nitrogen gas adsorption−desorption isotherms for MNP-MSN NPs. (B) Pore size distribution obtained from adsorption measurements.

temperature was measured at 37 and 42 °C, and the data are presented in Figure 7.

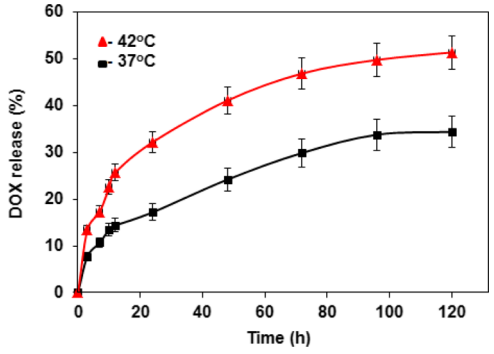

Figure 7. Release profile of DOX from MNP-MSN-PF-127 at 37 and 42 °C.

It is observed that during the first 24 h at 37 °C, the release of DOX was predominant and reached around 17.2%, and thereafter, a power law release pattern was observed. This might be due to a combined effect of the physically adhered drug and the drug present in the mesoporous structure. However, when the temperature was raised to 42 °C, the release of DOX was significantly increased from 17.2 to 32.2% for 24 h and reached up to 51.4% for 120 h. This must be due to a collapsed structure of PF-127. This is expected because the LCST of PF-127 is close to 42 °C. From this, it can be concluded that the block copolymer of PF-127 demonstrated the combined and complementary role of the stimuli-responsive drug-delivery carrier where the PF-127 segment was responsible for the fabrication of thermoresponsive MNP-MSN-PF-127-Tf at body temperature (37 °C). The externally coated PPF-127 effectively delayed the release of DOX from the mesopores of silica under physiological conditions such as temperature 37 °C and pH 7.4, suggesting that the nanocarrier developed (MNP-MSN-PF-127-Tf) here is a potential candidate for the delivery of drugs. Thus, the sustained drug release improves the accumulation of DOX at the tumor site while enhancing the anticancer efficiency.

To investigate the nature of the release mechanism, we have fitted the in vitro DOX release data in an empirical relation[38−40]

$$\frac{M_t}{M_\infty} = Kt^n \quad (1)$$

where M_t and M_∞ are the cumulative DOX release from the NPs at time t and ∞, respectively. The parameters n and k were estimated by the method of least squares at the 95% confidence limit, and these data are presented in Table 1. The

Table 1. DOX Release Mechanism Determined from the Korsmeyer−Peppas Model

temperature in °C	n	k	release mechanism
37	0.6175	0.165	non-Fickian (anomalous)
42	0.6589	0.182	non-Fickian (anomalous)

parameter k represents the extent of interaction between the DOX and NPs. The exponent n represents the nature of the release mechanism. For instance, if $n \leq 0.45$, it corresponds to the Fickian mechanism. For anomalous behavior, the value of n lies between 0.5 and 0.75 (i.e., it slightly deviates from the Fickian trend). In the present study, the obtained values of n vary from 0.6175 to 0.6589. Thus, the release of DOX from the NPs was found to follow an anomalous type of behavior.[40−42]

2.3. In Vitro Cytotoxicity of Drug-Loaded NPs. To assess the cytotoxicity of the drug-loaded NPs in U87 cells, the MTT assay was performed under various conditions at 48 and 96 h, and the results thus obtained are presented in Figure 8A,B, respectively.

It is observed that the cytotoxicity of the drug-loaded NPs is dependent on the drug concentration and the treatment period. The determined IC_{50} values of the blank NPs, DOX-MNP-MSN-PF-127, DOX-MNP-MSN-PF-127 with external magnetic field, DOX-MNP-MSN-PF-127-Tf, DOX-MNP-MSN-PF-127-Tf with external magnetic field, and DOX for 48 h were found to be 121.98, 60.96, 43.69, 0.57, 0.172, and 0.051 μg/mL, respectively; and for 96 h, they were 106.33, 52.69, 38.49, 0.074, 0.039, and 0.015 μg/mL, respectively. The data revealed that DOX-MNP-MSN-PF-127-Tf exhibited significantly lower IC_{50} values as compared to blank NPs, indicating its potential anticancer effect. This can be attributed to the presence of drugs and Tf in the mesoporous NPs. However, the IC_{50} value was found to be substantially low because of the application of an external magnetic field, highlighting the importance of the external magnetic field in the application of these NP conjugates. Obviously, the enhanced cytotoxicity effect is due to the influence of the magnetic field, which favors the binding of MNPs on the cells, and therefore, the percentage of cell viability decreased. At 96 h, a significant cytotoxicity effect was observed when compared

DOI: 10.1021/acsomega.8b00152
ACS Omega 2018, 3, 8017−8026

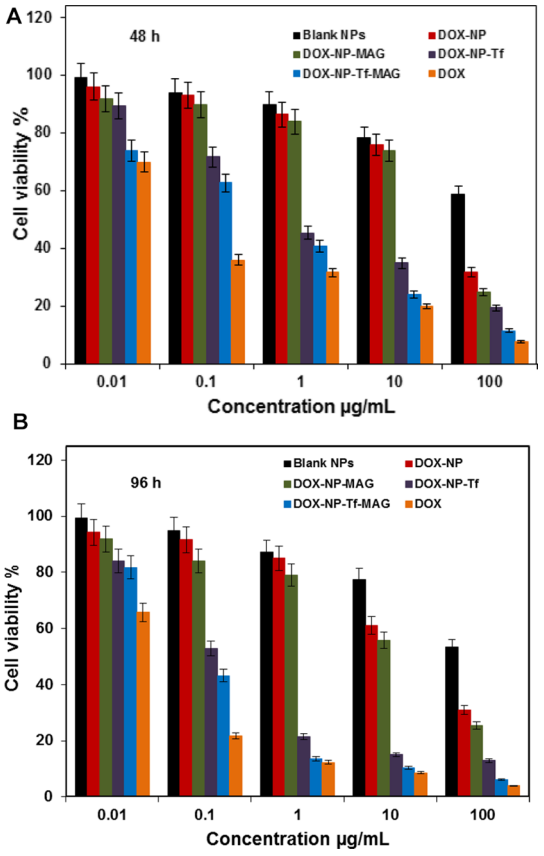

Figure 8. (A) Viability of U87 cells after treatment with blank NPs, free drug (DOX), DOX-MNP-MSN-PF-127 (DOX-NP), DOX-MNP-MSN-PF-127 with external magnetic field (DOX-NP-MAG), DOX-MNP-MSN-PF-127-TF (DOX-NP-Tf), and DOX-MNP-MSN-PF-127-Tf with external magnetic field (DOX-NP-Tf-MAG) at 48 h. (B) Viability of U87 cells after treatment with blank NPs, free drug (DOX), DOX-MNP-MSN-PF-127 (DOX-NP), DOX-MNP-MSN-PF-127 with external magnetic field (DOX-NP-MAG), DOX-MNP-MSN-PF-127-TF (DOX-NP-Tf), and DOX-MNP-MSN-PF-127-Tf with external magnetic field (DOX-NP-Tf-MAG) at 96 h.

to 48 h, and this effect might be due to a longer treatment period. The blank NPs did not show any noticeable cytotoxicity even at 1.0 μg/mL concentration. However, some effect on the cell viability was noticed when the concentration of NPs reached beyond 1.0 μg/mL.

2.4. Drug Uptake Studies in U87 Cells. The uptake of the drug-loaded NPs in U87 cells was quantified using a flow cytometer, and the data thus obtained are presented in Figure 9. The geometric-mean fluorescence intensities of DOX in the cells treated with DOX, DOX-MNP-MSN-PF-127-Tf, and DOX-MNP-MSN-PF-127-Tf with external magnetic field were found to be 2462, 7940, and 13791, respectively. To compare the data, the geometric mean fluorescence intensity of the untreated cells (control) was also determined and is shown in Figure 9. From the data, it is observed that the cells treated with DOX-MNP-MSN-PF-127-Tf conjugates showed a significant increase in the fluorescence intensity as compared to DOX. This is due to the presence of Tf protein, which itself helps to bind the DOX-MNP-MSN-PF-127-Tf conjugates with U87 cell lines. Similarly, the fluorescence intensity increased further when the external magnetic field was applied. This again signifies the importance of the external magnetic field as observed in cell viability results.

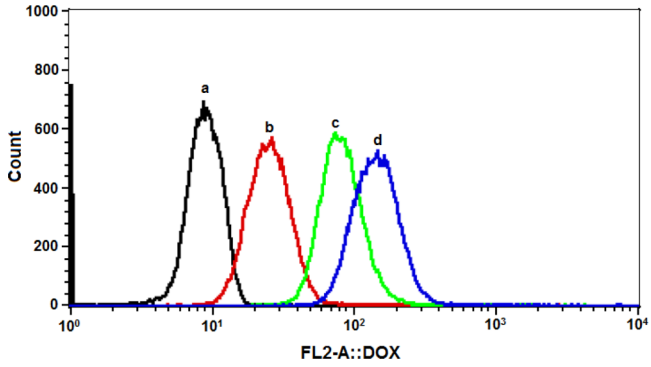

Figure 9. Flow cytometric analysis of U87 cells after treatment with (a) control, (b) DOX, (c) DOX-MNP-MSN-PF-127-Tf, and (d) DOX-MNP-MSN-PF-127-Tf with external magnetic field at a concentration 5 μg/mL for 4 h. DOX intensity is denoted as FL2-A.

2.5. In Vitro Drug Uptake Studies in U87 across the BBB Model. Targeting the brain or the CNS is a major challenge for designing the therapeutics to address the neuronal pathology. Only 5% of the drugs listed in the comprehensive medicinal chemistry database target the CNS, and this is mainly due to the intact and complex structure of the BBB.[43] To mimic the permeability of NPs through a tightly intact BBB, an in vitro model was established using HBME cell lines. A two-chamber transwell system was separated by the membrane as a barrier on which HBME cells were cultured. The HBME cells were incubated with 5 μg/mL test drug (DOX), DOX-MNP-MSN-PF-127, DOX-MNP-MSN-PF-127 with external magnetic field, DOX-MNP-MSN-PF-127-Tf, and DOX-MNP-MSN-PF-127-Tf with external magnetic field for 4 h at 37 °C, and their corresponding fluorescence intensities were measured using a flow cytometer, and the results thus obtained are presented in Figure 10. From the data, we have estimated the geometric mean fluorescence intensity for DOX, DOX-MNP-MSN-PF-127, DOX-MNP-MSN-PF-127 (with magnetic field), DOX-MNP-MSN-Tf, and DOX-MNP-MSN-Tf (with magnetic field), and the values are found to be 4296, 4993, 5037, 5968, and 56747, respectively. It is explicitly indicated that in the presence of the BBB model, the cells treated with DOX-MNP-MSN-PF-127-Tf showed a higher drug uptake compared to the cells treated with DOX. The higher uptake of DOX-MNP-MSN-PF-127-Tf by the HBME cells is due to a combined interaction of PF-127 and Tf on the cell membrane. The PF-127 polymer is known to promote active membrane transport, whereas Tf enhances the cellular uptake of the drug-loaded NPs. This is expected because the Tf-Rs are proven to overexpress in both the brain capillary endothelium and glioma cells. Though the BBB was present, cells treated with DOX-MNP-MSN-Tf in the presence of a magnetic field showed the highest accumulation of DOX among the five experimental groups.

3. CONCLUSIONS

In this study, we have systematically synthesized the DOX-loaded magnetic mesoporous NPs. These were subsequently coupled with PF-127 followed by conjugation with Tf so as to achieve the sustained release of drugs at the targeted site. The size and shape of the NPs determined by DLS and TEM were adequate and suitable for crossing the BBB. The magnetic saturation of the developed NPs was found to be 26.10 emu/g, indicating that even after coating with the silica and polymer,

DOI: 10.1021/acsomega.8b00152
ACS Omega 2018, 3, 8017−8026

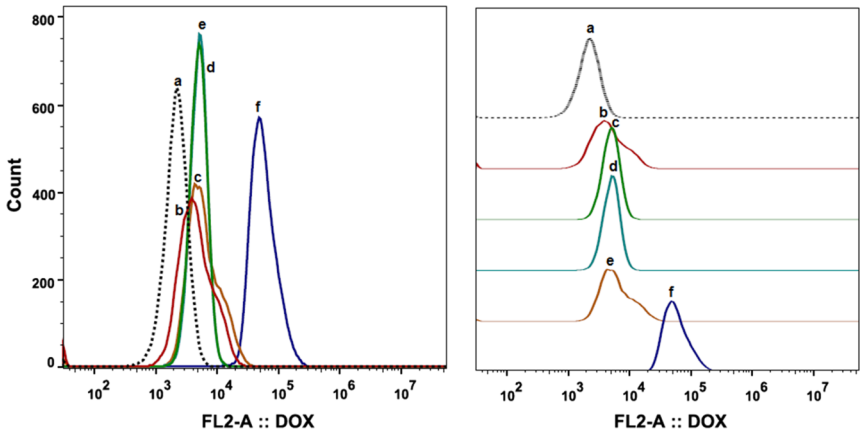

Figure 10. Flow cytometric analysis of U87 cells after treatment with (a) control, (b) DOX, (c) DOX-MNP-MSN-PF-127, (d) DOX-MNP-MSN-PF-127 with external magnetic field, (e) DOX-MNP-MSN-PF-127-TF, and (f) DOX-MNP-MSN-PF-127-TF with external magnetic field in the BBB model at 5 μg/mL concentration for 4 h. DOX intensity is denoted as FL2-A.

the NPs sufficiently retained their magnetic property. The cytotoxicity assay clearly indicated that the Tf-conjugated NPs (DOX-MNP-MSN-PF-127-Tf) exhibited a significantly lower IC_{50} value (0.570 μg/mL) at 37 °C for 48 h as compared to the blank NPs (121.98 μg/mL). This is due to the presence of drugs and Tf in the NPs. Thus, the functionalized nanocarriers developed here sensibly recognize and bind to U87 cells selectively. From the in vitro study, it is clearly suggested that DOX-MNP-MSN-PF-127-Tf exhibited a much higher anticancer activity and permeability across the BBB than the free DOX, and therefore, glioma cells undergo apoptosis through receptor-mediated transcytosis. Further, in the presence of magnetic field, DOX-MNP-MSN-PF-127-Tf enhanced its permeability across the BBB, and thereby a satisfactory efficacy was achieved in regard to the antiglioblastoma activity. On the basis of the results, we anticipate that nanocarriers (DOX-MNP-MSN-PF-127-Tf) developed in this investigation provide an effective strategy to target and antagonize the glioblastoma by successfully crossing the BBB.

4. EXPERIMENTAL SECTION

4.1. Materials and Methods. Iron(III) chloride hexahydrate ($FeCl_3 \cdot 6H_2O$, 98%), iron(II) chloride tetrahydrate ($FeCl_2 \cdot 4H_2O$), ammonium hydroxide (NH_4OH, 28−30%), TIPB (96%), decane (99%), NHS (98%), EDC, SA, triethylamine (TEA), 4-dimethylaminopyridine (DMAP), dimethyl sulfoxide (DMSO), holo-Tf, and DOX in the form of hydrochloride salt were purchased from Sigma-Aldrich, Chemie, GmbH, Germany. OA (99%), TEOS (98%), APTES (98%), cetyltrimethylammonium bromide (99%), and EG (anhydrous, 98%) were procured from TCI Chemicals, Japan. All the chemicals were of reagent grade and used as received. Deionized Millipore water was used throughout the experiments.

4.2. Synthesis of MNPs. Magnetic iron NPs were synthesized using the co-precipitation method.[44] Briefly, 30 mL of 0.1 M $FeCl_3$ and 15 mL of 0.1 M $FeCl_2$ solutions were mixed and heated at 80 °C for 10 min under constant stirring in a nitrogen atmosphere. To this, 3 mL of 5 M ammonium hydroxide was added and stirred further at the same temperature for 30 min. To obtain sterically stabilized MNPs, 100 μL of OA (23 wt %) was added drop-wise to the solution and stirred for 30 min. The resulting mixture was subsequently incubated at 80 °C for 50 min. The mixture was then heated to 110 °C so as to evaporate the excess ammonium hydroxide and water. The black precipitate thus obtained was washed several times with deionized water and followed by acetone to remove the excess OA. Each time, washing was removed by magnetic decantation, and finally, it was subjected to lyophilization to obtain the stabilized MNPs in a powder form. The synthetic protocols for the preparation of MNPs are presented in Scheme 1.

4.3. Synthesis of MNP-MSNs. The mesoporous silica MNPs were synthesized using the modified method.[45] Briefly, 25 mg of stabilized MNPs were dispersed in 2 mL of chloroform, and the entire solution was poured into a beaker containing 17 mL of 0.4 M CTAB solution. The resulting mixture was sonicated at 50 °C for 30 min to obtain a homogeneous microemulsion, and this was further heated to 70 °C and incubated for 15 min under stirring to evaporate the residual chloroform. The MNPs were subsequently transferred into a solution, consisting of 50 mL water, 17 mL of EG, and 1.2 mL of NH_4OH, and kept for heating at 70 °C for 10 min under stirring. To create the pores in the NPs, 1.77 mL of decane and 0.725 mL of TIPB were added to the resulting mixture and stirred for 2 h at the same temperature. Decane was added 2 h prior to TIPB. To this, 0.5 mL of TEOS was added drop-wise with constant stirring for 3 h at 70 °C and cooled. The product thus obtained was washed and lyophilized and designated as MNP-MSNs. The reaction is shown in Scheme 2.

4.4. DOX Loading and Amine Functionalization. To load the DOX into MNP-MSNs, the organic surfactant was removed initially by dissolving 60 mg of MNP-MSNs in 60 mL ethanol containing 160 mg of ammonium nitrate at 60 °C and kept for 30 min. The product thus obtained was washed with ethanol and water, centrifuged, and dried. Out of the resulting quantity, 15 mg of MNP-MSNs was suspended in ethanol. The suspension was then mixed with 10 mg of DOX and stirred for 24 h under dark conditions. The surface of the MNP-MSNs was then functionalized with amino groups by adding 2.5 μL of APTES to the drug-loaded suspension while stirring for 8 h at room temperature. The functionalized drug-loaded NPs were then isolated and subjected to centrifugation to remove the excess APTES. The supernatant was analyzed using a UV−vis spectrophotometer at 480 nm to estimate the extent of drug loading and encapsulation. The loading of drug and amine functionalization is presented in Scheme 3.

DOI: 10.1021/acsomega.8b00152
ACS Omega 2018, 3, 8017−8026

4.5. End-Group Modification of Pluronic F-127. The end-group modification of PF-127 was carried out by dissolving 1.4 g of anhydrous PF-127 in 25 mL of 1,4 dioxane followed by the addition of 26 mg of SA, 30 mg of DMAP, and 32 mL of TEA. The mixture was stirred under N_2 atmosphere for 24 h at room temperature. After evaporation of the solvent, a white residue was obtained. This residue was then dissolved in 40 mL of chloroform to remove the unreacted SA by filtration. The collected transparent filtrate was precipitated by adding excess cold diethyl ether batch-wise. The precipitate so obtained was dried under vacuum and stored for later use. The preparation of end-group modification is presented in Scheme 4.

4.6. Synthesis of MNP-MSN-PF-127. Before the conjugation of PF-127 to DOX-loaded MNP-MSNs, the modified PF-127 was cross-linked with EDC. The EDC is an efficient cross-linking agent for the polymers having carboxyl groups, which is being used to activate the carboxyl groups toward the formation of amide or ester. Briefly, 40 mg of modified PF-127 and 90 mg of EDC together with 52 mg of NHS were dissolved in 5 mL of water and stirred for 6 h. To this aqueous dispersion, amino-functionalized MNP-MSN NPs (50 mg particles in 10 mL of water) were added, and the pH of the mixture was adjusted to 5.8. The mixture was kept in an oven oscillator (150 rpm) for 72 h at room temperature. The resulting drug-loaded nanocarriers were washed several times with distilled water, centrifuged, freeze-dried, and stored for further use. The reaction process of drug-loaded nanocarriers is presented in Scheme 5.

4.7. Conjugation of Tf on Drug-Loaded Nanocarriers. To conjugate the Tf to drug-loaded nanocarriers, 10 mg of drug-loaded MNP-MSN-PF-127 was dispersed in the mixture containing 5 mL of PBS, 250 μL of EDC (1 mg/mL), and 250 μL of NHS (1 mg/mL). The resulting mixture was stirred at room temperature for 4 h to create amine-reactive esters on the carboxylic acid−terminated PF-127. Using EDC and NHS, Tf was conjugated to MNP-MSN-PF-127 from the reaction that occurred between the −COOH groups of PF-127 and $-NH_2$ groups on Tf molecules. The nanocarriers thus obtained were dispersed in 2 mL of PBS. To this mixture, 100 μL of Tf (1 mg/mL) was added drop-wise and stirred for 2 h, and later it was incubated at 4 °C overnight. The composite NPs were collected by centrifugation and washed several times with water to remove the unreacted species. Finally, the product was lyophilized and stored at 4 °C. The synthesis of Tf-conjugated drug-loaded nanocarriers is shown in Scheme 6.

4.8. Characterization of NPs. The modified NPs with different functionalities were characterized using an FTIR spectrometer (Nicolet, Impact-410, USA). The particle size and the zeta potential of the modified NPs were determined using a zeta-sizer (Anton-Paar, Litesizer 500, USA). On the basis of the DLS principle, light-scattering measurements were performed using a laser of wavelength 658 nm at a 90° scattering angle. Samples were prepared by dispersing the modified NPs in deionized water (0.5 mg/mL) at 25 °C. The diameter and morphology of the modified NPs were also visualized using TEM (JEOL, Tokyo, Japan). The samples were prepared by dispersing the modified NPs (500 mg/mL) in Millipore water employing ultrasonication for 3 min. One drop of this suspension was deposited carefully on a 300 mesh carbon-coated TEM copper grid and air-dried at room temperature. Thermal stability of the modified NPs was assessed in the temperature range of 25−800 °C using TGA (TGA Q 20, TA Instruments, Waters LLC, USA) at a heating rate of 10 °C/min under nitrogen (100 mL/min) atmosphere. The magnetic saturation of MNP-MSNs-PF-127 was evaluated using a vibrating sample magnetometer (Lakeshore VSM 7410, USA) at room temperature. Nitrogen adsorption−desorption isotherms obtained were used to calculate the pore size distribution and the specific surface area using BJH and BET (BET surface area analyzer, Micromeritics, Japan) after removing the CTAB template. The concentration of DOX was determined using a UV−vis spectrophotometer (Hitachi U-2800, Japan).

4.9. Drug Loading and in Vitro Release Study. Before performing the drug-release study, the EE and loading content (LC) of the drug in the developed NPs were respectively determined using eqs 2 and 3.

$$\text{EE of drug (\%)} = (\text{Initial amount of drug used} - \text{Amount of drug in supernatant}) / (\text{Initial amount of drug used}) \times 100 \quad (2)$$

$$\text{LC of drug (\%)} = (\text{Initial amount of drug used} - \text{Amount of drug in supernatant}) / (\text{Amount of NPs used}) \times 100 \quad (3)$$

The in vitro drug release study was performed in triplicates at two different temperatures of 37 and 42 °C. Briefly, 10 mg of drug-loaded NPs was dispersed in 5 mL of pH 7.4 PBS solution containing 0.05% (w/v) of Tween 80. The resulting mixture was allowed to stir at 37 and 42 °C separately by keeping in an incubator shaker. At different time intervals, 1 mL of the supernatant was removed from each solution and then replaced by adding the same volume of fresh PBS. The concentration of DOX was estimated by measuring its absorbance at a fixed wavelength of 480 nm.

4.10. Cell Culture. The human primary glioblastoma cell line (U87 MG) was procured from the National Centre for Cell Science (NCCS, Pune, India), and HBME cells were procured from Cell Systems (Washington, USA). The cells were grown in Dulbecco's modified Eagle's medium with 10% fetal bovine serum and 1% penicillin−streptomycin in a humidified incubator at 37 °C and 5% CO_2.

4.11. In Vitro Cytotoxicity Assay of Drug-Loaded Nanocarriers. The cytotoxic effect of blank NPs, DOX-MNP-MSN-PF-127-Tf, DOX-MNP-MSN-PF-127-Tf with external magnetic field, and free DOX was determined using the MTT assay, based on the reduction of (3-[4,5-dimethylthiazol-2-yl]-2,5-diphenyltetrazolium bromide) to formazan in metabolically viable cells. Briefly, U87 cells were seeded onto 96-well plates at a density of approximately 5000 cells per well. On the following days, the cells were treated with different concentrations (0.01, 0.1, 1.0, 10, and 100 μg/mL) of blank NPs, DOX-MNP-MSN-PF-127, DOX-MNP-MSN-PF-127 with external magnetic field, DOX-MNP-MSN-PF-127-Tf, DOX-MNP-MSN-PF-127-Tf with external magnetic field, and DOX. The cells were cultivated in the presence of an external magnetic field using a magnet placed under each well plate. After 24 h of incubation, the cells were washed with PBS to remove the unbound drug and replaced with a fresh growth medium. The cell viability was determined using Cell Titer 96 Non-Radioactive Cell Proliferation Assay. Dye solution (50

DOI: 10.1021/acsomega.8b00152
ACS Omega 2018, 3, 8017−8026

μL) was added to 100 μL of the medium in each well. The plates were gently shaken and incubated for 4 h at 37 °C under 5% CO_2 atmosphere. The supernatant was removed and 100 μL of DMSO was added, and the plates were gently shaken to solubilize the formed formazan. The absorbance was then measured with a microplate spectrophotometer at 540 nm.

4.12. Cellular Internalization of NPs. The cellular uptake of NPs, such as DOX-MNP-MSN-PF-127-Tf, DOX-MNP-MSN-PF-127-Tf with external magnetic field, and DOX, was determined using a flow cytometer. In brief, U87 cells were seeded onto a six-well culture plate or slide flask at a density of 3×10^5 cells/2 mL and incubated in a CO_2 incubator at 37 °C for 24 h. Later, the cells were treated with DOX-MNP-MSN-PF-127-Tf, DOX-MNP-MSN-PF-127-Tf with external magnetic field, and DOX (5 μg/mL) at 4 h in a humidified CO_2 incubator at 37 °C. The untreated cells were used as a control. After treatment, the cells were washed twice with PBS to remove the unbound NPs followed by trypsinization and resuspension in 500 μL of PBS. Flow cytometric analysis was carried out in a DOX channel employing an FL2-A detector (Becton Dickinson, BD Accuri C6, USA). All the results were expressed in terms of mean fluorescence intensity.

4.13. Drug Uptake across the BBB Using an in Vitro Model. The BBB model was established using a method previously described by Cui et al.[46] A 0.2% gelatin solution was used to precoat the trans-well inserts, which was then aspirated out, and the inserts were allowed to dry in a biosafety cabinet hood for 1 h. The HBME cells were seeded at a density of 1×10^5 cells per well and incubated for 7 days. The growth medium was changed every 2 days. After 7 days, the transendothelial electrical resistance value of the BBB was measured using EVOM and EVOMX Epithelial Voltohmmeters (World Precision Instruments, Inc., FL, USA) and was found to be 250 Ω cm^2. The inserts containing cultured HBME cells were then transferred to a six-well plate containing 24 h old cultured U87 cells. The medium was aspirated from the inserts containing the HBME cells. These cells were treated with the required concentration of test compounds (5 μg/mL) in 2 mL of culture medium and incubated for 4 h. One of the wells was left untreated and was considered as a negative control. At the end of the treatment, the inserts were removed from the six-well plates, and the medium was transferred into 15 mL centrifuge tubes. The centrifuged mass was washed with 500 μL of PBS. Subsequently, the PBS solution was removed and 200 μL of trypsin−EDTA solution was added to it, and this was incubated at 37 °C for 5 min. The culture medium was poured back into their respective wells, and the cells were harvested directly into the centrifuge tubes. The cells were subsequently washed with 1 mL of 1× D-PBS and subjected to centrifugation at 300*g*, and the separated D-PBS was discarded. Following this, 0.5 mL (2%) of paraformaldehyde was added to the cells and incubated at room temperature for 15 min, which was later centrifuged at 300*g* to discard the solution. Again, the cells were washed with 1 mL of 1× D-PBS and subjected to centrifugation at 300*g* and the separated D-PBS was discarded. Finally, 500 μL of D-PBS was added and mixed thoroughly to have a dispersed cell suspension, which was immediately subjected to a flow cytometer analysis using an FL2-A detector.

AUTHOR INFORMATION

Corresponding Author

*E-mail: mahadevappayk@gmail.com. Phone: +91-9448590765. Fax: +91-836-2771275 (M.Y.K).

ORCID

Mahadevappa Y. Kariduraganavar: 0000-0002-2159-0543

Notes

The authors declare no competing financial interest.

ACKNOWLEDGMENTS

The authors sincerely acknowledge the financial support of the UGC, New Delhi, under the UPE-FAR-I Program [grant no. 14-3/2012(NS/PE)] and the DST, New Delhi, under the DST-PURSE-Phase-II Program [grant no. SR/PURSE Phase 2/13(G)]. G.B.H. sincerely acknowledges the UPE-FAR-I Program for extending the fellowship to pursue the Ph.D. program.

REFERENCES

(1) Rock, K.; McArdle, O.; Forde, P.; Dunne, M.; Fitzpatrick, D.; O'Neill, B.; Faul, C. A clinical review of treatment outcomes in glioblastoma multiforme the validation in a non-trial population of the results of a randomized Phase III clinical trial: has a more radical approach improved survival? *Br. J. Radiol.* **2014**, *85*, e729−e733.

(2) Ohka, F.; Natsume, A.; Wakabayashi, T. Current trends in targeted therapies for glioblastoma multiforme. *Neurol. Res. Int.* **2012**, *2012*, 1−13.

(3) Thakkar, J. P.; Dolecek, T. A.; Horbinski, C.; Ostrom, Q. T.; Lightner, D. D.; Barnholtz-Sloan, J. S.; Villano, J. L. Epidemiologic and molecular prognostic review of glioblastoma. *Cancer Epidemiol., Biomarkers Prev.* **2014**, *23*, 1985−1996.

(4) Gan, C. W.; Feng, S.-S. Transferrin-conjugated nanoparticles of Poly(lactide)-d-α-Tocopheryl polyethylene glycol succinate diblock copolymer for targeted drug delivery across the blood-brain barrier. *Biomaterials* **2010**, *31*, 7748−7757.

(5) Lu, W.; Tan, Y.-Z.; Hu, K.-L.; Jiang, X.-G. Cationic albumin conjugated pegylated nanoparticle with its transcytosis ability and little toxicity against blood-brain barrier. *Int. J. Pharm.* **2005**, *295*, 247−260.

(6) Nie, S.; Xing, Y.; Kim, G. J.; Simons, J. W. Nanotechnology applications in cancer. *Annu. Rev. Biomed. Eng.* **2007**, *9*, 257−288.

(7) Ferrari, M. Cancer nanotechnology: opportunities and challenges. *Nat. Rev. Cancer* **2005**, *5*, 161−171.

(8) Peer, D.; Karp, J. M.; Hong, S.; Farokhzad, O. C.; Margalit, R.; Langer, R. Nanocarriers as an emerging platform for cancer therapy. *Nat. Nanotechnol.* **2007**, *2*, 751−760.

(9) Schroeder, A.; Heller, D. A.; Winslow, M. M.; Dahlman, J. E.; Pratt, G. W.; Langer, R.; Jacks, T.; Anderson, D. G. Treating metastatic cancer with nanotechnology. *Nat. Rev. Cancer* **2012**, *12*, 39−50.

(10) Ashley, C. E.; Carnes, E. C.; Phillips, G. K.; Padilla, D.; Durfee, P. N.; Brown, P. A.; Hanna, T. N.; Liu, J.; Phillips, B.; Carter, M. B.; Carroll, N. J.; Jiang, X.; Dunphy, D. R.; Willman, C. L.; Petsev, D. N.; Evans, D. G.; Parikh, A. N.; Chackerian, B.; Wharton, W.; Peabody, D. S.; Brinker, C. J. The targeted delivery of multicomponent cargos to cancer cells by nanoporous particle-supported lipid bilayers. *Nat. Mater.* **2011**, *10*, 389−397.

(11) Li, C. A targeted approach to cancer imaging and therapy. *Nat. Mater.* **2014**, *13*, 110−115.

(12) Mulvey, J. J.; Villa, C. H.; McDevitt, M. R.; Escorcia, F. E.; Casey, E.; Scheinberg, D. A. Self-assembly of carbon nanotubes and antibodies on tumours for targeted amplified delivery. *Nat. Nanotechnol.* **2013**, *8*, 763−771.

(13) Slowing, I. I.; Trewyn, B. G.; Giri, S.; Lin, V. S.-Y. Mesoporous silica nanoparticles for drug delivery and biosensing applications. *Adv. Funct. Mater.* **2007**, *17*, 1225−1236.

DOI: 10.1021/acsomega.8b00152
ACS Omega 2018, 3, 8017−8026

(14) Hendrix, M. J. C.; Seftor, E. A.; Hess, A. R.; Seftor, R. E. B. Molecular plasticity of human melanoma cells. *Oncogene* **2003**, *22*, 3070−3075.
(15) Sun, N.-F.; Meng, Q.-Y.; Tian, A.-L.; Hu, S.-Y.; Wang, R.-H.; Liu, Z.-X.; Xu, L. Nanoliposome-mediated FL/TRAIL double-gene therapy for colon cancer: in vitro and in vivo evaluation. *Cancer Lett.* **2012**, *315*, 69−77.
(16) Pankhurst, Q. A.; Connolly, J.; Jones, S. K.; Dobson, J. Applications of magnetic nanoparticles in biomedicine. *J. Phys. D: Appl. Phys.* **2003**, *36*, R167−R181.
(17) Chen, F.-H.; Zhang, L.-M.; Chen, Q.-T.; Zhang, Y.; Zhang, Z.-J. Synthesis of a novel magnetic drug delivery system composed of doxorubicin-conjugated Fe3O4 nanoparticle cores and a PEG-functionalized porous silica shell. *Chem. Commun.* **2010**, *46*, 8633−8635.
(18) Guan, Y.-Q.; Zheng, Z.; Huang, Z.; Li, Z.; Niu, S.; Liu, J.-M. Powerful inner/outer controlled multi-target magnetic nanoparticle drug carrier prepared by liquid photo-immobilization. *Sci. Rep.* **2014**, *4*, 4990.
(19) Zhan, X.; Guan, Y.-Q. Design of magnetic nanoparticles for hepatocellular carcinoma treatment using the control mechanisms of the cell internal nucleus and external membrane. *J. Mater. Chem. B* **2015**, *3*, 4191−4204.
(20) Dilnawaz, F.; Singh, A.; Mohanty, C.; Sahoo, S. K. Dual drug loaded superparamagnetic iron oxide nanoparticles for targeted cancer therapy. *Biomaterials* **2010**, *31*, 3694−3706.
(21) Hua, M.-Y.; Liu, H.-L.; Yang, H.-W.; Chen, P.-Y.; Tsai, R.-Y.; Huang, C.-Y.; Tseng, I.-C.; Lyu, L.-A.; Ma, C.-C.; Tang, H.-J.; Yen, T.-C.; Wei, K.-C. The effectiveness of a magnetic nanoparticle-based delivery system for BCNU in the treatment of gliomas. *Biomaterials* **2011**, *32*, 516−527.
(22) He, Q.; Shi, J. MSN anti-cancer nanomedicines: chemotherapy enhancement, overcoming of drug resistance, and metastasis inhibition. *Adv. Mater.* **2014**, *26*, 391−411.
(23) Chen, Y.; Chen, H.; Shi, J. In vivo bio-safety evaluations and diagnostic/therapeutic applications of chemically designed mesoporous silica nanoparticles. *Adv. Mater.* **2013**, *25*, 3144−3176.
(24) He, L.; Huang, Y.; Zhu, H.; Pang, G.; Zheng, W.; Wong, Y.-S.; Chen, T. Cancer-targeted monodisperse mesoporous silica nanoparticles as carrier of ruthenium polypyridyl complexes to enhance theranostic effects. *Adv. Funct. Mater.* **2014**, *24*, 2754−2763.
(25) He, L.; Chen, T.; Yu, Y.; Hu, H.; Zheng, W.; Kwong, W.-L.; Zou, T.; Che, C.-M. A cancer-targeted nanosystem for delivery of gold(III) complexes: enhanced selectivity and apoptosis-inducing efficacy of a gold(III) porphyrin complex. *Angew. Chem., Int. Ed.* **2014**, *53*, 12532−12536.
(26) Simond, M. R.; Ballerat-Busserolles, K.; Coulier, Y.; Rodier, L.; Coxam, J.-Y. Dissociation Constants of Protonated Amines in Water at Temperatures from 293.15 K to 343.15 K. *J. Solution Chem.* **2012**, *41*, 130−142.
(27) Gupta, A. K.; Gupta, M. Synthesis and surface engineering of iron oxide nanoparticles for biomedical applications. *Biomaterials* **2005**, *26*, 3995−4021.
(28) Lee, H.; Yu, M. K.; Park, S.; Moon, S.; Min, J. J.; Jeong, Y. Y.; Kang, H.-W.; Jon, S. Thermally cross-linked superparamagnetic iron oxide nanoparticles: synthesis and application as a dual imaging probe for cancer in vivo. *J. Am. Chem. Soc.* **2007**, *129*, 12739−12745.
(29) Wei, Z.; Hao, J.; Yuan, S.; Li, Y.; Juan, W.; Sha, X.; Fang, X. Paclitaxel-loaded Pluronic P123/F127 mixed polymeric micelles: Formulation, optimization and in vitro characterization. *Int. J. Pharm.* **2009**, *376*, 176−185.
(30) Kabanov, A. V.; Batrakova, E. V.; Miller, D. W. Pluronic block copolymers as modulators of drug efflux transporter activity in the blood-brain barrier. *Adv. Drug Delivery Rev.* **2003**, *55*, 151−164.
(31) Yue, J.; Liu, S.; Wang, R.; Hu, X.; Xie, Z.; Huang, Y.; Jing, X. Transferrin-Conjugated Micelles: Enhanced Accumulation and Antitumor Effect for Transferrin-Receptor-Overexpressing Cancer Models. *Mol. Pharm.* **2012**, *9*, 1919−1931.
(32) Ojima, I. Modern molecular approaches to drug design and discovery. *Acc. Chem. Res.* **2008**, *41*, 2−3.
(33) Thorpe, P. E. Vascular targeting agents as cancer therapeutics. *Clin. Cancer Res.* **2004**, *10*, 415−427.
(34) Parren, P. W.; van de Winkel, J. G. An integrated science-based approach to drug development. *Curr. Opin. Immunol.* **2008**, *20*, 426−430.
(35) Li, H.; Qian, Z. M. Transferrin/transferrin receptor-mediated drug delivery. *Med. Res. Rev.* **2002**, *22*, 225−250.
(36) Visser, C. C.; Stevanović, S.; Heleen Voorwinden, L.; Gaillard, P. J.; Crommelin, D. J. A.; Danhof, M.; de Boer, A. G. Validation of the Transferrin Receptor for Drug Targeting to Brain Capillary Endothelial CellsIn Vitro. *J. Drug Targeting* **2004**, *12*, 145−150.
(37) Chen, S.; Li, Y.; Guo, C.; Wang, J.; Ma, J.; Liang, X.; Yang, L.-R.; Liu, H.-Z. Temperature-Responsive Magnetite/PEO−PPO−PEO Block Copolymer Nanoparticles for Controlled Drug Targeting Delivery. *Langmuir* **2007**, *23*, 12669−12676.
(38) Kulkarni, S. B.; Kariduraganavar, M. Y.; Aminabhavi, T. M. Molecular migration of aromatic liquids into a commercial fluoroelastomeric membrane at 30, 40, and 50°C. *J. Appl. Polym. Sci.* **2003**, *90*, 3100−3106.
(39) Korsmeyer, R. W.; Gurny, R.; Doelker, E.; Buri, P.; Peppas, N. A. Mechanisms of solute release from porous hydrophilic polymers. *Int. J. Pharm.* **1983**, *15*, 25−35.
(40) Paul, D. R.; McSpadden, S. K. Diffusional release of a solute from a polymer matrix. *J. Membr. Sci.* **1976**, *1*, 33−48.
(41) Riger, P. L.; Peppas, N. A. A simple equation for description of solute release II. Fickian and anomalous release from swellable devices. *J. Controlled Release* **1987**, *5*, 37−42.
(42) Peppas, N. A. Analysis of Fickian and non-Fickian drug release from polymers. *Pharm. Acta Helv.* **1985**, *60*, 110−111.
(43) Lin, J.-J.; Chen, J.-S.; Huang, S.-J.; Ko, J.-H.; Wang, Y.-M.; Chen, T.-L.; Wang, L.-F. Folic acid-Pluronic F127 magnetic nanoparticle clusters for combined targeting, diagnosis, and therapy applications. *Biomaterials* **2009**, *30*, 5114−5124.
(44) Mohapatra, S.; Mallick, S. K.; Maiti, T. K.; Ghosh, S. K.; Pramanik, P. Synthesis of highly stable folic acid conjugated magnetite nanoparticles for targeting cancer cells. *Nanotechnology* **2007**, *18*, 385102−385111.
(45) Zhang, J.; Li, X.; Rosenholm, J. M.; Gu, H.-C. Synthesis and characterization of pore size-tunable magnetic mesoporous silica nanoparticles. *J. Colloid Interface Sci.* **2011**, *361*, 16−24.
(46) Cui, Y.; Xu, Q.; Chow, P. K.-H.; Wang, D.; Wang, C.-H. Transferrin-conjugated magnetic silica PLGA nanoparticles loaded with doxorubicin and paclitaxel for brain glioma treatment. *Biomaterials* **2013**, *34*, 8511−8520.

DOI: 10.1021/acsomega.8b00152
ACS Omega 2018, 3, 8017−8026